



# Neural-network-based automatic trajectory adaptation for quality characteristics control in powder compaction

Hoomaan MoradiMaryamnegari<sup>1</sup> · Seif-El-Islam Hasseni<sup>1</sup> · Elias Ganthaler<sup>1</sup> · Thomas Villgrattner<sup>2</sup> · Angelika Peer<sup>1</sup>

Received: 6 June 2023 / Accepted: 4 November 2023  
© The Author(s) 2023

## Abstract

Future manufacturing systems will have to become more intelligent to be able to guarantee a constantly high quality of products while simultaneously reducing labor-intensive quality-assurance tasks to address the shortage in workforce. In this work, we study the application of neural networks to the field of powder metallurgy and more specifically the production of green parts as part of a typical sintering process. More specifically, we explore the usage of neural-network-based predictions in closed-loop control. We train neural networks based on a series of produced workpieces, and use these networks in closed-loop production to predict quality characteristics like weight and dimensions of the workpiece in real-time. Based on these predictions an adaptive trajectory planner adjusts then trajectory key points and with this the final piston trajectories to bring and keep quality characteristics of workpieces within tolerance. We finally compare the control performance of this neural network-based approach with a pure sensor-based approach. Results indicate that both approaches are able to bring and keep quality characteristics within their tolerance limits, but that the neural network-based approach outperforms the sensor-based approach in the transient phase, whereas in steady state the neural network needed to be updated from time to time to reach the same high performance as the sensor-based approach. Since updating needs to be performed only from time to time, required expensive sensors can be shared among multiple machines and thus, costs can be reduced. At the same time the superior prediction performance of the neural-network-based approach in transient phases can be exploited to accelerate setting up times for new workpieces. Future work will target the automation of the recording of the training dataset, the exploration of further machine learning methods as well as the integration of additional sensor data to further improve predictions.

**Keywords** Trajectory key-point adaptation · Neural network prediction · Powder metallurgy · Data-driven estimation and control

## Introduction

Sintered workpieces made out of iron-based metal powder are characterized by a wide range of shapes, high-dimensional accuracy up to IT10, and high surface quality with energy-efficient and cost-effective production in large quantities (Beiss, 2013; Schatt et al., 2007; Klocke, 2015; van der Haven et al., 2022; Kumar et al., 2021; Krok and Wu, 2017; Evans and De Jonghe, 2016; Wilson et al., 2019; Manivannan et al., 2021; O’Flynn and Corbin, 2019). The needed compaction pressure is provided by press machines consisting of several independent punch levels able to follow predefined trajectories. To guarantee the same constant quality of produced workpieces over a long period of time, regular quality checks and manual trajectory adjustments are needed

---

✉ Angelika Peer  
Angelika.Peer@unibz.it  
Hoomaan MoradiMaryamnegari  
Hoomaan.MoradiMaryamnegari@student.unibz.it  
Seif-El-Islam Hasseni  
SeifElIslam.Hasseni@unibz.it  
Elias Ganthaler  
Elias.Ganthaler@student.unibz.it  
Thomas Villgrattner  
Thomas.Villgrattner@gknpm.com

<sup>1</sup> Human-centered Technologies and Machine Intelligence Lab, Faculty of Engineering, Free University of Bozen-Bolzano, Bolzano 39100, Bz, Italy

<sup>2</sup> GKN Powder Metallurgy, Brunico 39031, Bz, Italy

to account for changing operating conditions due to e.g. varying temperature, humidity, stroke rate, or powder quality. Also the first setup of the machine requires manual measurements and iterative adjustments of trajectory key points. These adjustments, however, are very labour-intensive since automation of them is still in its infancy.

On the other hand, machine learning techniques have gained significant popularity over the last few years and are being applied in different fields of manufacturing (Liu et al., 2023), such as final product prediction (Wang et al., 2017), condition monitoring (Yu Pimenov et al., 2022), and process planning (Li et al., 2022). Since their data-driven approach allows for the development of real-time capable models, even in the absence of physical equations (Qin et al., 2023) or when related physical models show less accuracy, they can be applied effectively in real systems (Koutsoupakis et al., 2023).

For example, several papers address the application of machine learning techniques to the fabrication of metal workpieces. In Satterlee et al. (2022), for example, the authors investigated the ability to classify porosities from cross-sectional images of 3D-printed metal parts by comparing the classification performance of 6 machine learning methods. The problem of crack evolution in structures has been treated by a predictor based on a neural network in Long et al. (2021). In Lou et al. (2019) again, six types of machine learning algorithms were used to predict the best raw material that optimizes tensile strength and brittleness (which are related to the powder compactability) when adopting core/shell techniques. Finally, when compacting iron powder in Malik et al. (2022), a neural network algorithm was adopted to predict the surface roughness from the compaction pressure, composition, and sintering temperature.

## Challenges and contributions

While machine learning models have been successfully used in the literature to gain valuable insight into processes or to make predictions, these predictions often remained theoretical or were limited to post-process analyses (Sivasankaran et al., 2011; Massimo et al., 2023) and were not effectively used to directly and immediately influence the manufacturing process. This represents a significant research gap as using predictive models to trigger online adaptations has a strong potential to enhance process stability, reduce manual interventions, and improve overall efficiency and quality, especially in cases where real-time capable physical models that reflect reality with sufficient accuracy cannot be obtained. Thus, while existing research has laid the foundation by demonstrating that machine learning algorithms can successfully predict various variables in a manufacturing context, there remains a clear need for further investigations on how these predictions can be integrated into automation

systems to enable automatic adjustments. In this paper which builds upon our previous work (Ganthaler et al., 2023), we aim to fill this gap by demonstrating how predictions generated by machine learning algorithms can be effectively used for online adjustment of trajectory key points to bring and keep quality characteristics within tolerances, thus advancing the state of the art in sintered part production.

In doing so, we follow the workflow sketched in Fig. 1. After having instrumented the press with proper sensors, we record a training dataset which is subsequently used for training the neural network models. Next, these models are implemented on the press allowing to obtain online predictions of the quality characteristics mass and dimensions. We further foresee an algorithm that updates the network models offline based on information obtained from recent workpieces if environmental conditions change and estimates become inaccurate. Finally, the obtained predictions are used to adapt trajectory key-points to bring and keep the quality characteristics within pre-defined tolerances. To assess the estimation and control performance, we compare the introduced system experimentally to a classical sensor-based baseline following an experimental design that allows to study transient as well as steady-state performance.

The paper is structured as follows: In Sect. “Materials and methods” a description of the machine and the studied workpieces is provided, as well as the quality characteristic estimators are described. The applied specialties for the sensor-based and neural-network-based implementations are reported in Sect. “Implementation”. The achieved estimation as well as control performance are presented and discussed in Sect. “Results”. Finally, the paper concludes in Sect. “Conclusion”.

## Materials and methods

### The press

The press machine used in experiments is a hydraulic powder press with three lower-level punches, respectively Lower Level 1 (LL1), Lower Level 2 (LL2), and Lower Level 3 (LL3), one core-rod (pin, CR), a fixed die, and two upper-level punches, respectively Top-ram (TR), and Upper Level 2 (UL2). Each level is actuated by hydraulic cylinders and can therefore move independently. The main cylinder of the top-ram can apply a maximum force of 700 kN and has two rapid traverse cylinders installed, allowing to move faster in free space. The first upper level is fixed on the top-ram. The second upper level is also mounted on the top-ram but has an additional actuator and can therefore move relatively to the top-ram. The tool-mounting mechanism is conically designed so that the pistons from levels below can move independently (see (1) in Fig. 2). Besides the pistons, an electrical

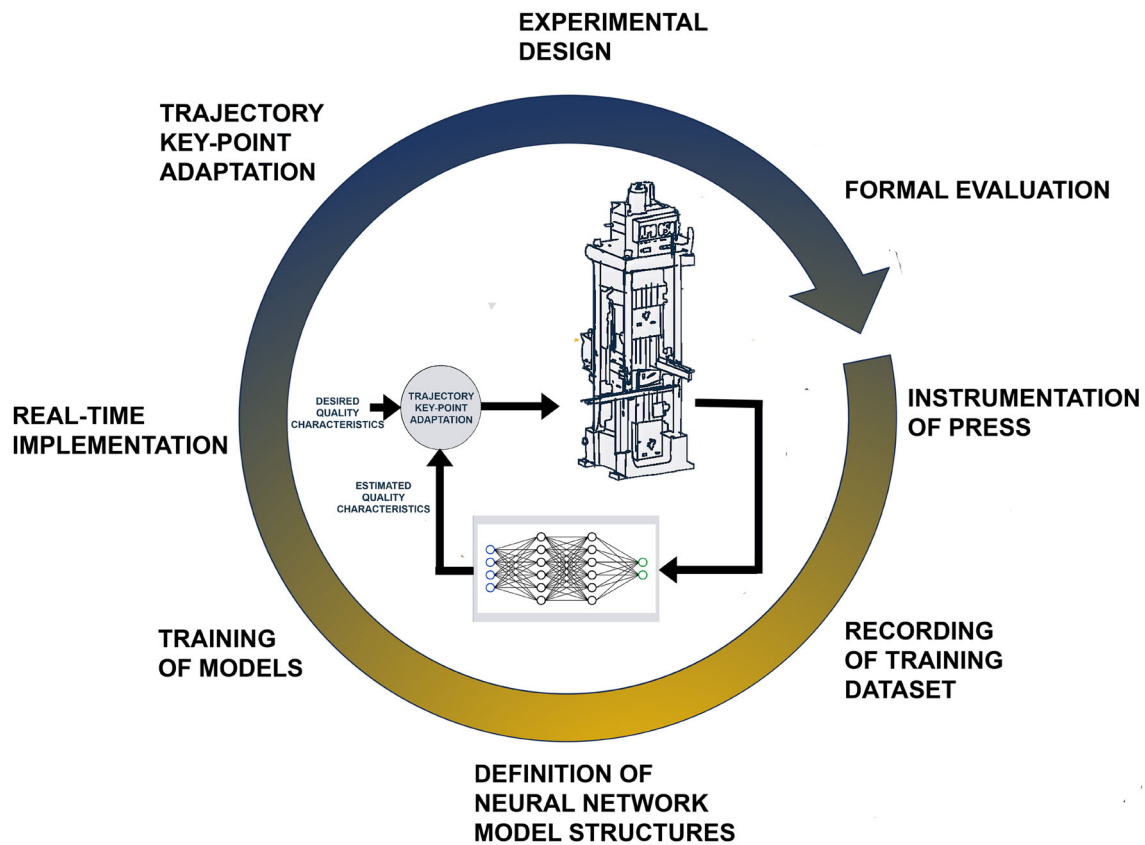


Fig. 1 Adopted workflow

servo motor is mounted and connected to the press moving the feeding shoe from its initial position towards the cavity. Additionally, there is a pick-and-place system, consisting of a gripper with three degrees of freedom (x-z-rotation) and an action (grasping). This gripper takes the produced green-part after being ejected from the press and places it on a scale. From there the workpiece is placed on a belt on which end a laser triangulation system measures the workpiece dimensions before it is finally loaded on a palletizer. The powder press is equipped with force sensing systems for each punch level and gauges for measuring the cylinder movement. The resolution of the position sensors is  $1\ \mu\text{m}$ , while the one of the force sensing system is below  $15\ \text{N}$ . All sensors are directly connected to dedicated interface boards of the main PLC of the powder press. The main PLC uses a sampling rate of  $2\ \text{kHz}$  to read out the sensors, run the low-level closed loop controllers, and send new set values to the valves actuating the hydraulic pistons. Furthermore, a graphical user interface is running on the main PLC, but with a much lower sampling rate. The set-up is further equipped with a scale with a resolution of  $1\ \text{mg}$  and a repeatability of  $2\ \text{mg}$  as well as a laser triangulation system with a linearity of  $\pm 0.006\%$  and a repeatability of  $0.4\ \mu\text{m}$ . The latter measures the geometrical dimensions of each produced workpiece using a laser

beam. Both measuring systems use their own dedicated sub PLCs. The communication between the main PLC and the sub PLCs is based on TCP/IP.

## Geometry of the workpieces and quality characteristics

### Workpiece 1

The first workpiece studied in the context of this work is a hollow cylinder with a total height of  $8.97\ \text{mm}$  and a flange height of  $2.99\ \text{mm}$ . Beside a die, two lower punch levels, a core rod, and one upper punch level are necessary for production. The quality characteristics considered for this workpiece are its mass as well as the length 1 and length 2, as shown in Fig. 3. Lower and upper control limits (LC, UC) and lower and upper tolerance limits (LT, UT) for this workpiece are detailed in Table 1.

### Workpiece 2

The second research workpiece, as shown in Fig. 4, is a multi-layer workpiece with three lower-levels and two

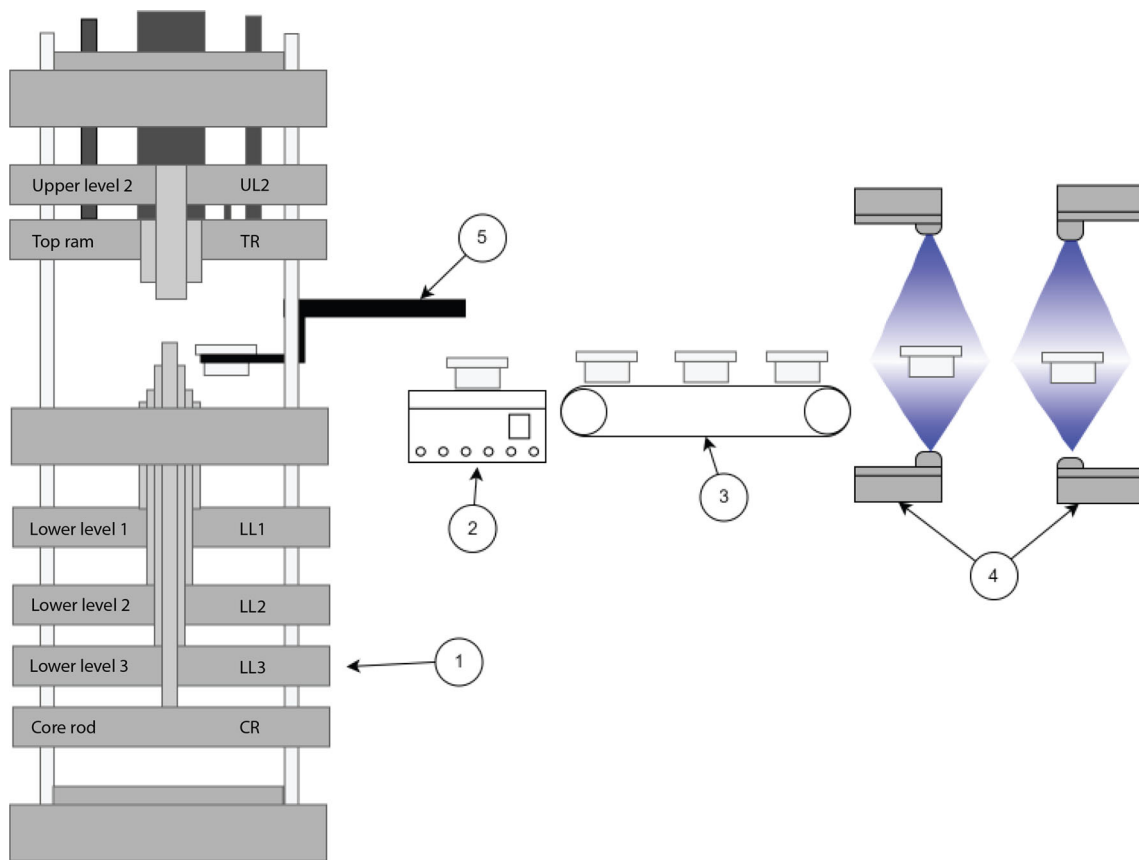


**Fig. 2** Setup of the production process: (1) press machine (2) weight scale (3) conveyor belt (4) laser triangulation system (5) pick-and-place system

**Fig. 3** First research workpiece

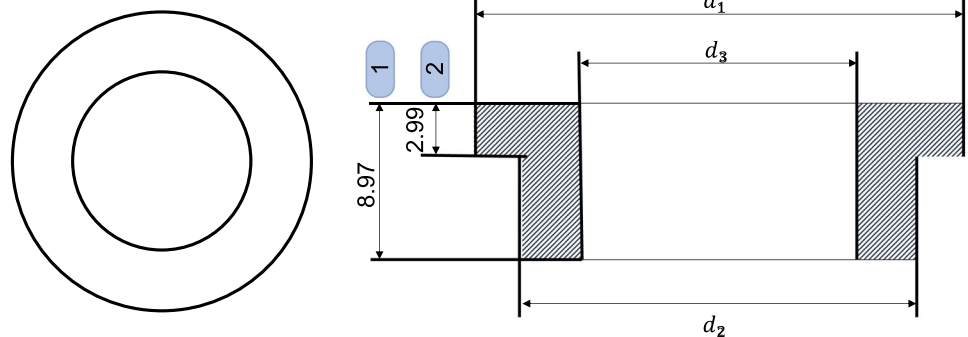


**Table 1** Tolerance limits for first research workpiece

| QC            | LT   | LC     | SET  | UC     | UT   |
|---------------|------|--------|------|--------|------|
| Mass [g]      | 16.2 | 16.25  | 16.4 | 16.55  | 16.6 |
| Length 1 [mm] | 8.92 | 8.9325 | 8.97 | 9.0075 | 9.02 |
| Length 2 [mm] | 2.94 | 2.9525 | 2.99 | 3.0275 | 3.04 |

upper-levels. The quality characteristics considered for this workpiece are its mass as well as the lengths 1 to 4 as shown in Fig. 4. Setpoint values as well as lower and upper control

limits (LC, UC) and lower and upper tolerance limits (LT, UT) for this workpiece are detailed in Table 2.

**Phases of production**

The green-part production can be divided into the following four main phases as shown in Fig. 5. During the *filling phase*, the filler moves from its initial position towards the cavity, which is formed by the lower-levels and the rigid die. By overpassing the cavity, the cavity gets filled with metal powder. To increase filling quality in terms of homogeneous filling

**Fig. 4** Second research workpiece

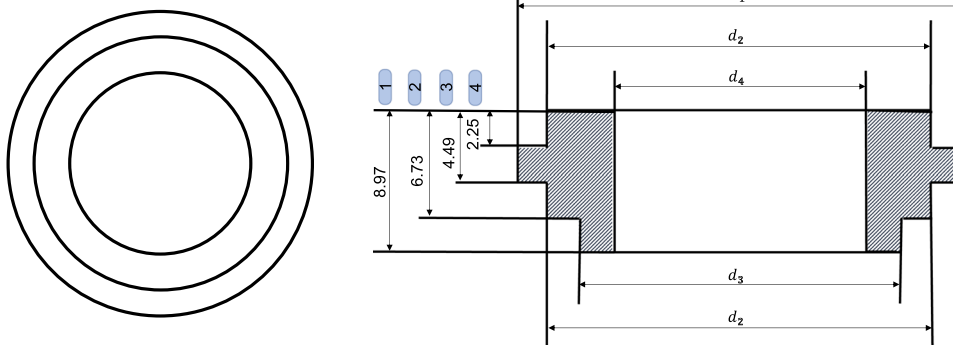


**Table 2** Tolerance limits for second research workpiece

| QC            | LT   | LC     | SET  | UC     | UT   |
|---------------|------|--------|------|--------|------|
| Mass [g]      | 16.1 | 16.15  | 16.3 | 16.45  | 16.5 |
| Length 1 [mm] | 8.92 | 8.9325 | 8.97 | 9.0075 | 9.02 |
| Length 2 [mm] | 6.68 | 6.6925 | 6.73 | 6.7675 | 6.78 |
| Length 3 [mm] | 4.44 | 4.4525 | 4.49 | 4.5275 | 4.54 |
| Length 4 [mm] | 2.2  | 2.2125 | 2.25 | 2.2875 | 2.3  |

density distribution, the filler can be commanded to perform wiggles with defined amplitude and frequency. Please note that the first green phase shows the end of the filling process of the current workpiece as well as the return of the filler to its start position, whereby the last green phase shows the initial filling phase of the next workpiece. The filling process ends and the *compaction phase* starts when the top-ram reaches the surface of the powder, which is marked in Fig. 5 by a horizontal line around an angular value of 0.55 s. During the compaction phase, all levels move towards each other till they reach the press position at 0.75 s. At this position, high-pressure loads are applied to the powder deforming it plastically. The compaction phase is followed by the *ejection phase*. During this phase, all lower levels move upwards, so that the produced green part can be grasped and transported by a robotic arm in the *removal phase*.

**Quality characteristics estimation**

**Workpiece 1**

Three neural networks were used as models for the estimation of selected quality characteristics such that each model had only one quality characteristic as output. We decided for multiple neural networks instead of a single one since from a practical implementation and maintenance point of view, it is desirable to define a single fixed-size network structure that generalizes over multiple types of workpieces. This allows one network to be implemented in the press software instead of customized ones that need to be adjusted every

time a new workpiece is added. Further, this way the time for offline training could be reduced and the estimation accuracy increased. Each model considered one hidden layer with 300 neurons and 18 features as input. In order to extract these features, the actual positions of the levels and forces measured during the compaction phase, were divided into three parts of equal size. Extracted position and force values are then averaged over each part to obtain the final features used as input to the neural network models.

**Training of Neural Networks** The data obtained during an experimental run was used for offline training of the neural network models. A dataset consisting of 1673 samples covering the three selected quality characteristics was used as training dataset. For obtaining this training dataset, the press parameters were changed manually to enforce situations with different initial conditions. But since at increased workpiece mass, a further decrease of dimensions can lead to high densities resulting in a high risk of damaging the compaction tool, only few workpieces with increased weight were produced.

For mass, values between 16.00 to 16.80 g were defined as the minimum and maximum admissible outputs of the neural network. For length 1, these values were defined to be 8.85 and 9.09 mm, whereas they were chosen to be 2.87 and 3.11 mm for length 2. These ranges were chosen based on values observed during a first rough settlement performed manually by skilled workers.

**Workpiece 2**

The chosen quality characteristics for the second workpiece are the mass, and four lengths. In analogy to workpiece 1, also for workpiece 2, neural networks were trained for each quality characteristic. Thus, in total five neural networks were used as black-box models to estimate the five quality characteristics. Each neural network considered one output and 30 features as input. Similarly to workpiece 1, the compaction section was divided into three parts and the mean of positions and forces for each of these parts was then used as input fea-

Fig. 5 The press cycle

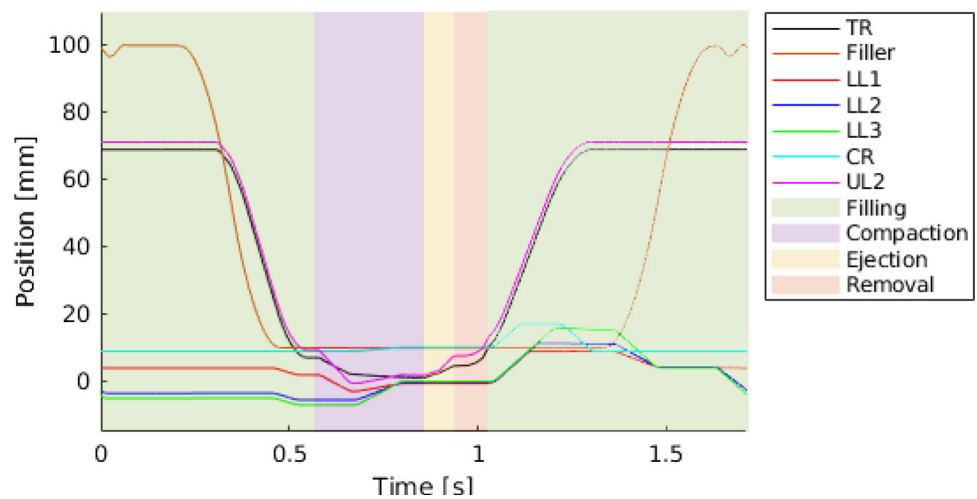


Table 3 Input features of the Neural Networks

| Input | Feature                                                             |
|-------|---------------------------------------------------------------------|
| 1     | Mean applied force by top-ram over first third of compaction phase  |
| 2     | Mean applied force by top-ram over second third of compaction phase |
| 3     | Mean applied force by top-ram over last third of compaction phase   |
| 4     | Mean top-ram position over first third of compaction phase          |
| 5     | Mean top-ram position over second third of compaction phase         |
| 6     | Mean top-ram position over last third of compaction phase           |
| 7     | Mean applied force by UL2 over first third of compaction phase      |
| 8     | Mean applied force by UL2 over second third of compaction phase     |
| 9     | Mean applied force by UL2 over last third of compaction phase       |
| 10    | Mean UL2 position over first third of compaction phase              |
| 11    | Mean UL2 position over second third of compaction phase             |
| 12    | Mean UL2 position over last third of compaction phase               |
| 13    | Mean applied force by LL1 over first third of compaction phase      |
| 14    | Mean applied force by LL1 over second third of compaction phase     |
| 15    | Mean applied force by LL1 over last third of compaction phase       |
| 16    | Mean LL1 position over first third of compaction phase              |
| 17    | Mean LL1 position over second third of compaction phase             |
| 18    | Mean LL1 position over last third of compaction phase               |
| 19    | Mean applied force by LL2 over first third of compaction phase      |
| 20    | Mean applied force by LL2 over second third of compaction phase     |
| 21    | Mean applied force by LL2 over last third of compaction phase       |
| 22    | Mean LL2 position over first third of compaction phase              |
| 23    | Mean LL2 position over second third of compaction phase             |
| 24    | Mean LL2 position over last third of compaction phase               |
| 25    | Mean applied force by LL3 over first third of compaction phase      |
| 26    | Mean applied force by LL3 over second third of compaction phase     |
| 27    | Mean applied force by LL3 over last third of compaction phase       |
| 28    | Mean LL3 position over first third of compaction phase              |
| 29    | Mean LL3 position over second third of compaction phase             |
| 30    | Mean LL3 position over last third of compaction phase               |



**Table 4** Parameters of neural networks

| Parameter                             | Value     |
|---------------------------------------|-----------|
| Percentage of training data           | 70        |
| Percentage of validating data         | 15        |
| Percentage of test data               | 15        |
| Number of hidden layers               | 1         |
| Number of neurons in the hidden layer | 300       |
| Estimation error goal                 | $10^{-8}$ |
| Maximum number of validation failures | 20        |
| Maximum number of epochs              | 1000      |

ture of the neural networks. More precisely, the input features for workpiece 2 are listed in Table 3.

**Training of Neural Networks** In order to train the neural networks, a dedicated dataset was captured that consists of 2417 samples. Again for obtaining this training dataset and to cover different initial conditions, the press parameters were changed manually.

For mass, values between 15.90 to 16.80 g were defined as the minimum and maximum admissible outputs of the neural network. For length 1, these values were defined to be 8.80 and 9.15 mm, whereas they were 6.50 and 6.95 mm for length 2, 4.35 and 4.64 mm for length 3, and 2.12 and 2.45 mm for length 4. The adopted parameters for defining the neural networks as well as training and validation data for both workpieces are shown in Table 4. The architecture of the Neural Networks for both workpieces is depicted in Fig. 6.

The computational times required for offline training of different networks on a PC equipped with a Core i9-10900E 2.8GHz CPU and 32GB of RAM are given in Table 5. When training five neural networks simultaneously in parallel, the maximum computation time amounts to 1085.9 s (needed for training network of mass).

### Updating of neural networks

Since over time, production conditions may change, the models originally trained under a specific condition may not maintain the same high accuracy over long time periods. To address this issue, it is necessary to update the networks from time to time using more recently produced workpieces. To determine whether an update is required, after producing a certain number of workpieces, the accuracy of the model can be checked. If the produced workpieces are found to be still within tolerance, the new online-captured dataset can be merged with the old one and models can be re-trained offline. This way, the accuracy of the estimations can be increased. If the produced workpieces are not anymore within tolerance

it is more advisable to only use the online dataset to re-train the neural networks to avoid to rely on very outdated data.

When the training is completed, the accuracy of the new model can be tested on an additional to-be-recorded test dataset. Only if the predictions of the new models are better than the old ones, the weights and biases of the old models are replaced by the new ones. The update process involving the recording of online and test datasets is explained in Fig. 7. The mentioned algorithm to update the models is described in detail in Algorithm 1.

---

### Algorithm 1: Online update algorithm.

---

```

Data: old neural network's weights and biases
p: number of produced workpieces for update
if number of produced workpieces == p then
  if the performance of the offline neural network is not desirable then
    | new dataset = online dataset
  end
  else
    | new dataset = online dataset + offline dataset
  end
  Split online dataset into 80% for training and 20% for validation
  Train neural network
  Test performance of neural network based on test set
  if the performance of the test set is better than offline neural network then
    | old weights = new weights
    | old biases = new biases
  end
  else
    | Continue with the offline neural network
  end
end

```

---

### Trajectory key-point adaptation

The implemented trajectory key-point adaptation scheme is shown in Fig. 8. To keep the quality characteristics mass and dimensions within tolerances the realized adaptation law modifies key points of the piston trajectories, which are related to the filling and press positions. Experiments were conducted with the aim of investigating the control performance of the introduced adaptive trajectory planner. As controlling all quality characteristics simultaneously may lead to high risks of destroying the punches, the following control sequences were adopted for each workpiece:

- Workpiece 1: Mass - Length 1 - Length 2
- Workpiece 2: Mass - Length 1 - Length 2 - Length 3 - Length 4

For all workpieces first the mass was brought into its tolerance limits and then the different lengths followed in a

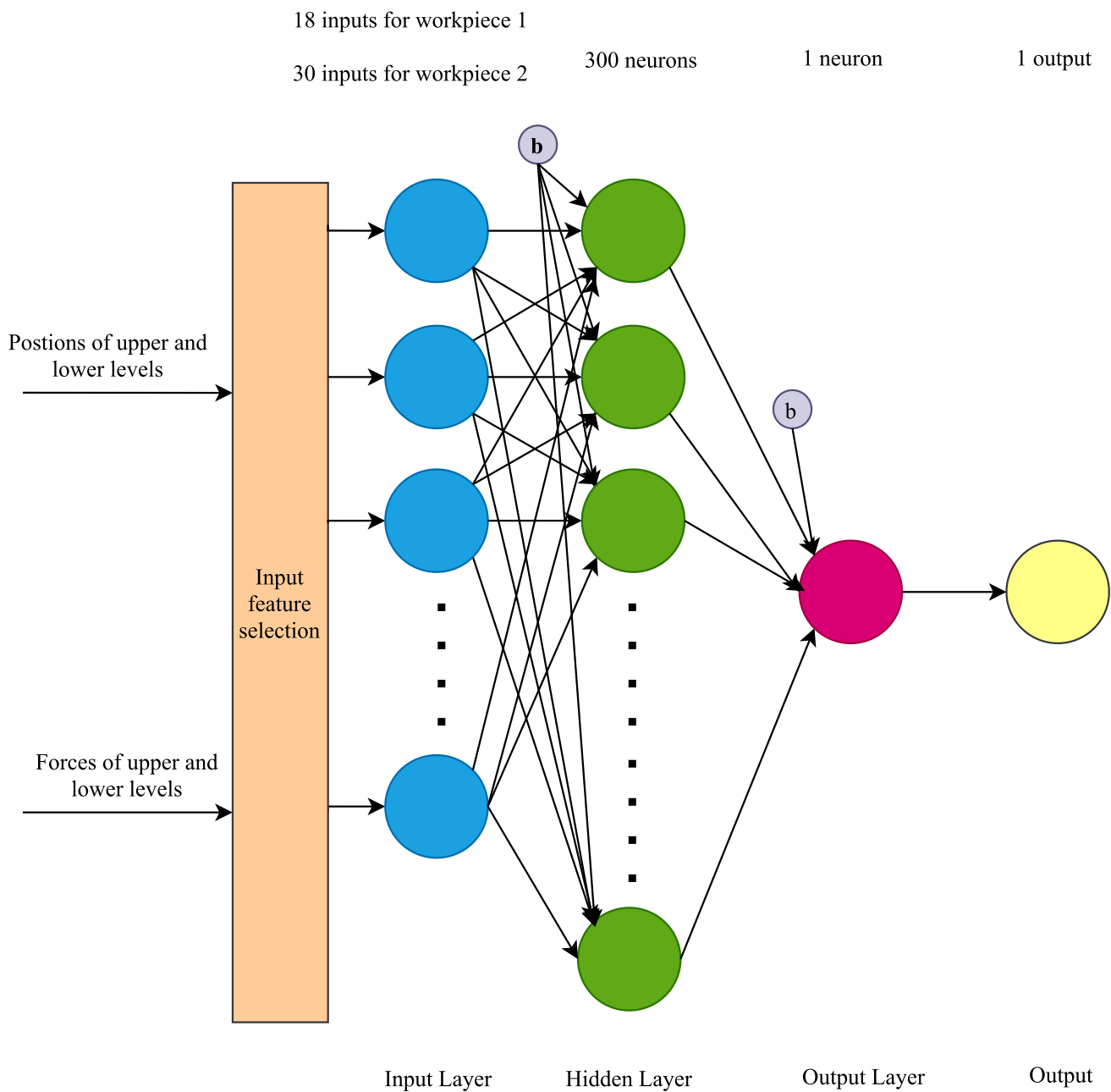


**Fig. 6** The neural network architecture for workpiece 1 and workpiece 2

**Table 5** Time required for offline training

| Network                                  | Time(sec)   |
|------------------------------------------|-------------|
| Network with only one output for Mass    | 1085.920130 |
| Network with only one output for Length1 | 488.337047  |
| Network with only one output for Length2 | 467.165505  |
| Network with only one output for Length3 | 424.296867  |
| Network with only one output for Length4 | 353.167252  |

cascaded order. Only once a specific estimated/measured dimension reached its predefined interval, the next quality characteristic was brought into tolerance.

#### Bringing mass into tolerance

When aiming for adjusting the mass of the workpiece, the height of the filling cavity or alternatively the filling density  $\rho_f$  can be changed. The new commanded filling density can be calculated with the rule of three as follows, assuming the



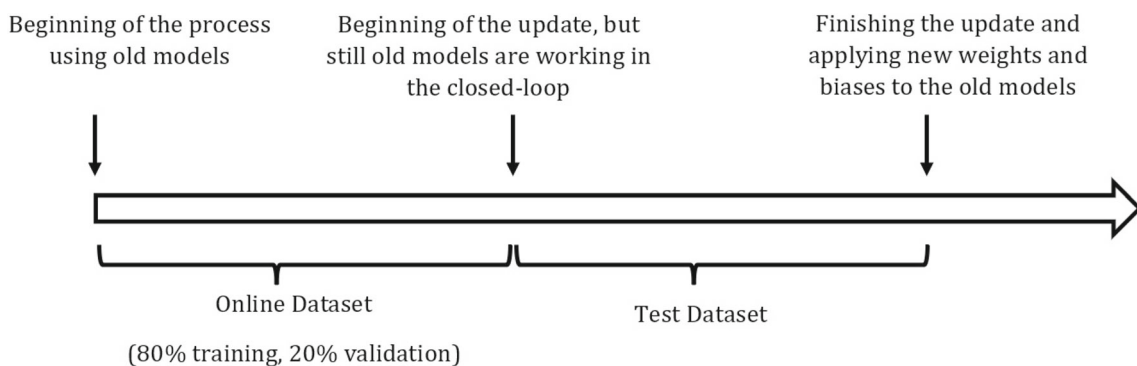


Fig. 7 The update process

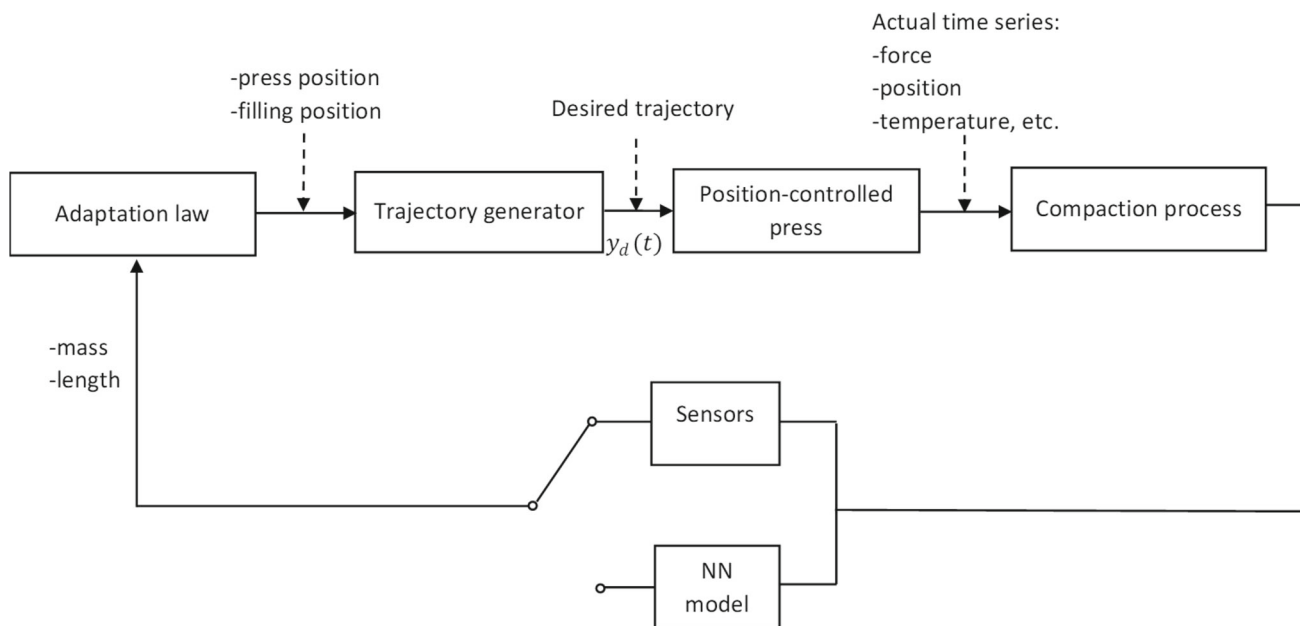


Fig. 8 Closed-loop control scheme

same final volume:

$$\rho_{f,new} = \rho_{f,old} \cdot \frac{m_{des}}{m_{old}} \tag{1}$$

To realize this new filling density, the volume of the cavity during the filling process is changed by the machine, which can be achieved by adjusting the filling positions, while the cross section remains the same due to the contour of the rigid die.

Hereby, filling density and filling height are linked with each other by the filling factor (FF), which can be calculated as follows:

$$FF = \frac{h_f}{h_{des}} = \frac{\rho_{des}}{\rho_f} \tag{2}$$

where  $h_f$  stands for the filling height,  $h_{des}$  for the final height of the workpiece and  $\rho_{des}$  for the desired mean density of the

final workpiece. An increased/decreased filling height results in an increased or decreased amount of powder that falls into the cavity. If the press positions remain unchanged, then the volume of the final workpiece remains the same, and thus, inevitably the mass and density of the workpiece increases or decreases accordingly.

**Bringing heights into tolerance**

The height of the workpiece can be controlled by changing the offset of each piston in press position. To reduce the height of the workpiece, the relative distance between the upper and lower pistons in press position has to be reduced. A positive delta at press position leads to an increased movement of the lower level and a reduced movement of the top-ram, while a negative delta to an increased vertical movement of the top-ram and a decreased vertical movement of the lower level. To change the press position, the controller has to read out

first the actual press position of the active pistons, excluding the core-rod. To keep the press-neutral zone and with this the area with minimal density at half the workpiece height, the applied pressure loads from both sides should be similar in magnitude. Thus, the top-ram and the lower level are changed according to a predefined ratio as follows:

$$x_{LL,new} = x_{LL,act} - k \Delta h, \quad (3)$$

$$x_{TR,new} = x_{TR,act} + (1 - k) \Delta h, \quad (4)$$

where  $x_{i,new}$  stands for the new press position,  $x_{i,act}$  for the actual set press position, and  $\Delta h$  for the error between desired and measured workpiece height. The weighted height-deviation  $\Delta h$  is added to the actual press-position of the upper-level and subtracted from the press-position of the lower-level pistons. The parameter  $k$  defines the share between lower and upper pistons.

## Implementation

The press is controlled by a standard PLC, while for testing purposes the software module with the neural network models and the adaptation law is running on an external PC. Hereby, the neural network model was implemented in Matlab/Simulink and a proprietary Simulink block provided by the PLC supplier was used to communicate with the press. In future, these models though would also need to be embedded into the PLC programme of the press. The sensor-based controller is implemented in Python and a Python-wrapper is used to establish the connection with the press PLC. Further, the following specialties apply for the individual implementations:

**Sensor-based controller:** A Python script controlling the workpiece quality characteristics reads all relevant data from the press. Each produced workpiece gets removed from the press, placed on a scale and then placed on a conveyor-belt before it passes the triangulation sensor. It takes seven workpieces or about 11 s (when producing at stroke rate 35) until the produced workpiece gets measured by the laser triangulation system (see Fig. 2). Therefore each quality measurement is saved in a ring-buffer and its median is used to control the different quality characteristics. Taking this and some safety margin into consideration, we decided to write every nine strokes new data to the press. To avoid sending measurements that may be considered outliers or wrong data, the measured height and mass are compared to the desired values with a pre-defined offset value.

**Black-box model-based controller:** The black-box models are implemented in MATLAB/Simulink using a Neural Network trained on a set of offline recorded data to estimate the

mass and height of every produced workpiece. To assure similar conditions as for the sensor-based controller, also every ninth stroke new data is sent to the press.

The Neural Network is designed in a way that it can be updated online. Therefore, crucial production data is stored continuously in a *.mat*-file, which can then be used to train the new neural network. The new generated biases and weights for the network are then used to update the adaptation law. The updating process can be activated at any time and requires about 120 strokes for determining the new network parameters.

## Results

In this section we first analyze the model estimation performance of the Neural Networks compared to the baseline based on sensors by starting from four initial conditions. Next, the control performance of sensor-based and model-based approaches are compared.

### Estimation performance

#### Workpiece 1

Aiming at evaluating the neural network models, a dedicated dataset recorded in open-loop with stroke rate 35 strokes/min was used. The dataset contains in total 872 samples. We changed the press parameters manually to cover a large set of values of the quality characteristics. Figure 9 shows the measured and estimated values of the quality characteristics (mass, length 1, and length 2) and Table 6 presents the estimation performance in terms of correlation, mean estimation error, standard deviation, and the root mean squared estimation-error (RMSE).

The neural network model of the first workpiece shows overall very good estimation performance predicting the three quality characteristics with an RMSE smaller than 0.04 g for the mass and 0.02 mm for the lengths 1 and 2. The observed mean estimation errors are  $2.1 \times 10^{-4}$  g for the mass,  $-0.0073$  mm and  $-0.004$  mm for lengths 1 and 2. In terms of correlations, the estimator reaches high correlations: 0.9714 for the mass, 0.98 and 0.976 for lengths 1 and 2, and thus, estimated values very well fit the shape of the measured quality characteristics.

#### Workpiece 2

Again, to evaluate the neural network estimators for the second workpiece, a dataset of 506 produced items was recorded in open-loop with 35 strokes/min. A large range of values of quality characteristics was covered by changing the press parameters manually. Figure 10 shows the measured and esti-

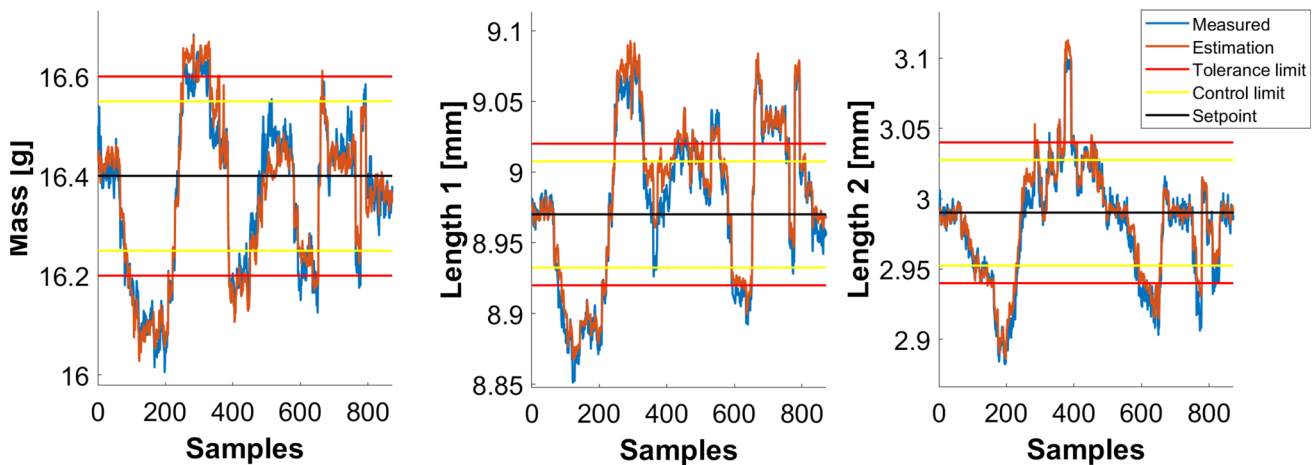


Fig. 9 Estimation performance of neural network model for a series of workpieces 1

**Table 6** Averaged estimation performance of the neural network model for workpiece 1

| QC       | Estimation performance (First workpiece) |                             |                 |                 |
|----------|------------------------------------------|-----------------------------|-----------------|-----------------|
|          | Mean error ( $\mu$ )                     | Std. deviation ( $\sigma$ ) | Correlation (R) | Estimation RMSE |
| Mass     | $2.1e-4$ g                               | 0.0385 g                    | 0.9714          | 0.0385 g        |
| Length 1 | -0.0073 mm                               | 0.0114 mm                   | 0.9800          | 0.0135 mm       |
| Length 2 | -0.0040 mm                               | 0.0088 mm                   | 0.9760          | 0.0097 mm       |

ated values of the quality characteristics (mass, lengths 1 to 4) and Table 7 presents the model performances in terms of correlation, mean estimation error, standard deviation, and the root mean squared estimation-error (RMSE).

The neural network model of the second workpiece shows overall very good estimation performance predicting the five quality characteristics with an RMSE smaller than 0.05 g for the mass and 0.02 mm for the lengths. The observed mean estimation errors are  $-0.0019$  g for the mass, 0.001 mm,  $-0.0012$  mm, and  $-4.3 \times 10^{-5}$  mm for lengths 1 to 4 respectively. In terms of correlations, the estimator reaches high correlations: 0.9692 for the mass, 0.9828, 0.9717, 0.9585, and 0.9547 for lengths 1 to 4 respectively, and thus, the estimated values very good fit the shape of the measured quality characteristics.

### Updating of neural networks

In Fig. 11, the proposed updating algorithm is applied to workpiece 1 in an experiment with initial conditions starting above tolerance for mass and both lengths. The first update is applied after producing 370 workpieces where jumps can be seen in the measurements and estimations. Although the accuracies of the estimations increase for all three quality characteristics, another update is applied at sample 516 to improve the estimation of both lengths, which also decreases the mass estimation error.

### Control performance

Next, we compare the control performance of the neural-network-based and sensor-based approach without considering updating the neural network models. As control sequence, the sequences indicated in Section 2.4 were adopted. Further, the following four different initial conditions were adopted, whereby each condition was repeated ten times:

- i.T.: both quality characteristics (mass and lengths) started within the predefined tolerance intervals
- b.T.: both quality characteristics started below tolerance
- a.T.: both quality characteristics started above tolerance
- c.T.: mass started below the tolerance limit and lengths above the tolerance limit

Please note that the case of mass starting above tolerance and lengths below was not considered, as at increasing workpiece mass further decreasing lengths can lead to high densities resulting in a high risk of damaging the compaction tools. To evaluate the control performance the following quality measures were adopted:

**Transient settling phase (Number of writing processes #W):** The controllers are tested with different initial conditions. To compare their capability to bring the quality characteristics within their predefined intervals, the number of writing operations #W required to bring the respective quality characteristics within their control limits is used.

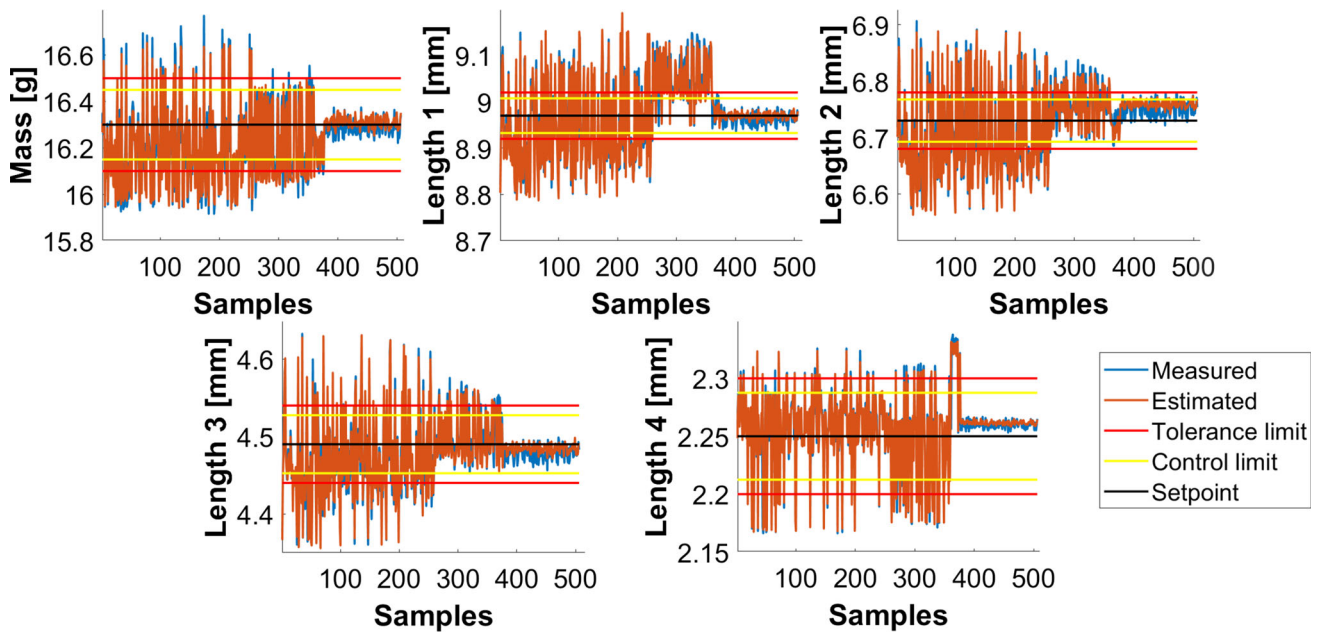


Fig. 10 Estimation performance of neural network model for a series of workpieces 2

Table 7 Averaged estimation performance of the neural network model for workpiece 2

| QC       | Model performance (Second workpiece) |                             |                 |                 |
|----------|--------------------------------------|-----------------------------|-----------------|-----------------|
|          | Mean error ( $\mu$ )                 | Std. deviation ( $\sigma$ ) | Correlation (R) | Estimation RMSE |
| Mass     | -0.0019 g                            | 0.0408 g                    | 0.9692          | 0.0408 g        |
| Length 1 | 0.0010 mm                            | 0.0156 mm                   | 0.9828          | 0.0156 mm       |
| Length 2 | 0.0012 mm                            | 0.0164 mm                   | 0.9717          | 0.0164 mm       |
| Length 3 | -0.0012 mm                           | 0.0135 mm                   | 0.9585          | 0.0135 mm       |
| Length 4 | -4.3e-5 mm                           | 0.0102 mm                   | 0.9547          | 0.0102 mm       |

**Steady-state phase (Root-mean-squared error (RMSE)):** The steady-state error has been determined by evaluating the root mean squared error considering the error between setpoint and measured quality characteristics over the last 30 produced workpieces.

### Workpiece 1

Figure 12 shows examples of measured mass, length 1, and length 2 of workpiece 1 resulting for the sensor-based approach, while Fig. 13 depicts them for the neural-network-based approach.

As can be seen, the quality characteristics take differently long till they enter the tolerance band and then fluctuate around their set points. Thus, average values obtained for each condition are used for comparison of the control approaches and are reported in Table 8 in terms of number of writing processes #W for the settling performance and the RMSE for the steady-state performance. We also report the average over all conditions for the RMSE, while we omit reporting the average over all conditions for settling due to

the large differences in values obtained for the different conditions.

As can be seen, in terms of settling, the neural-network-based control descriptively shows better performance for all the quality characteristics and all initial conditions. In terms of steady-state RMSE though, in general the sensors-based controller shows better performance.

Results of a statistical t-test performed on this data are reported in Table 9. Means as well as 95% confidence intervals are shown in Figs. 14 and 15. Concerning the RMSE in steady-state, the t-test performed on data averaged over all experiments showed significant differences at a significance level of 5% for all the quality characteristics with a significantly better performance of the sensor-based approach compared to the neural-network-based approach. In terms of settling performance, the different initial conditions had to be analyzed individually since averaging over all of them would have resulted in no significant results due to the large differences in the obtained values between conditions. When analyzing the initial conditions individually, the t-tests indicate that the neural-network-based approach leads to a

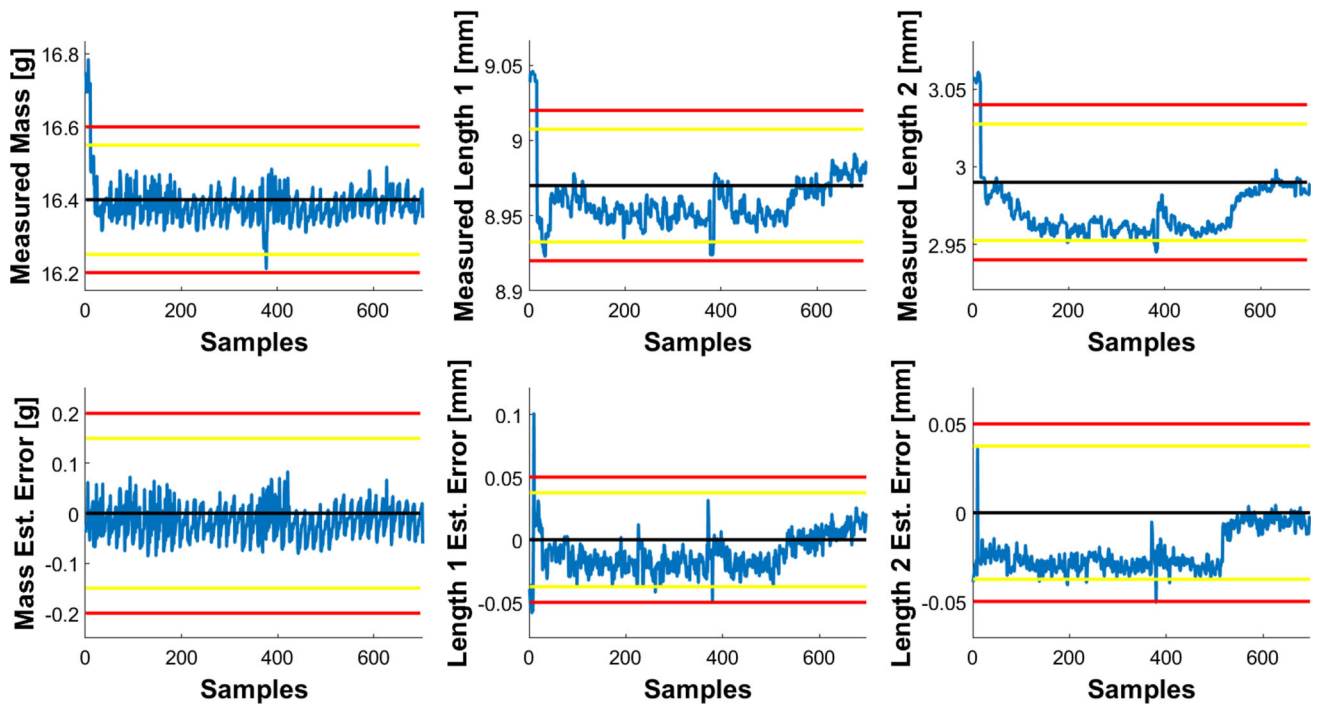


Fig. 11 Measured mass and lengths as well as estimation errors for workpiece 1 when using the proposed update algorithm

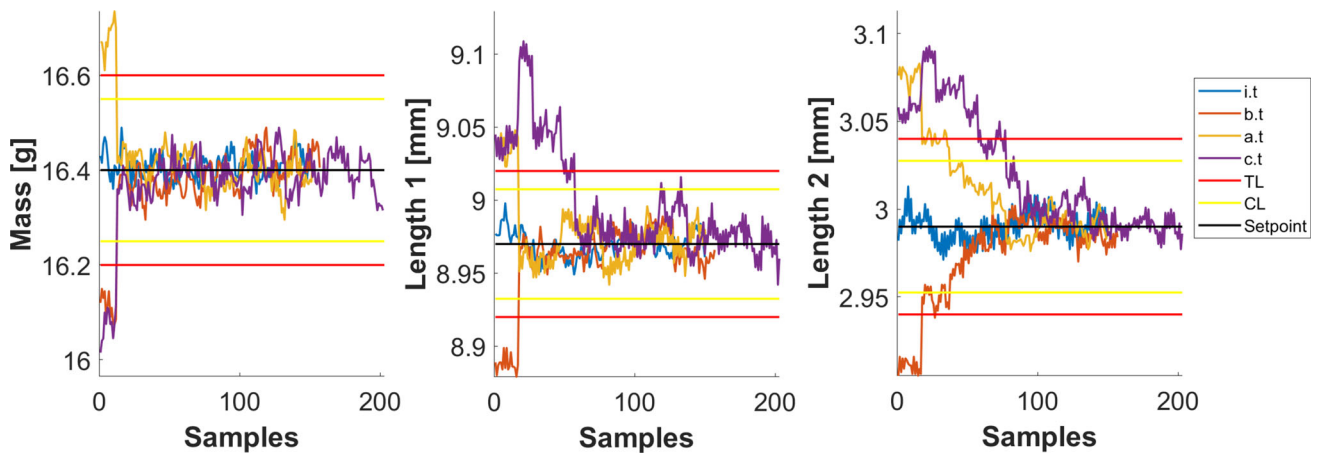


Fig. 12 Time-series of quality characteristics of workpiece 1 for control based on sensor measurements

significantly better control performance than the sensors-based approach when considering lengths. In terms of mass though, no significant difference could be found for all initial conditions.

**Workpiece 2**

In Figs. 16 and 17 examples of measured values of the quality characteristics mass, and lengths 1 to 4 of the second workpiece are shown for each of the initial conditions and for sensor-based as well as neural-network-based approach.

All the quality characteristics converge and stabilize within their tolerance limits. Table 10 summarizes the

observed control performance in terms of settling performance and steady-state performance. As can be observed, in terms of settling, the neural-network-based approach descriptively shows better performance for all the quality characteristics and all initial conditions, except for length 4 in the below tolerance initial condition. Also in terms of steady-state performance, in general the neural-network-based approach shows better performance for all quality characteristics except for mass.

Table 11 reports the results of the statistical analysis performed based on the aforementioned measurements. Figs. 18 and 19 show the means and the confidence intervals of



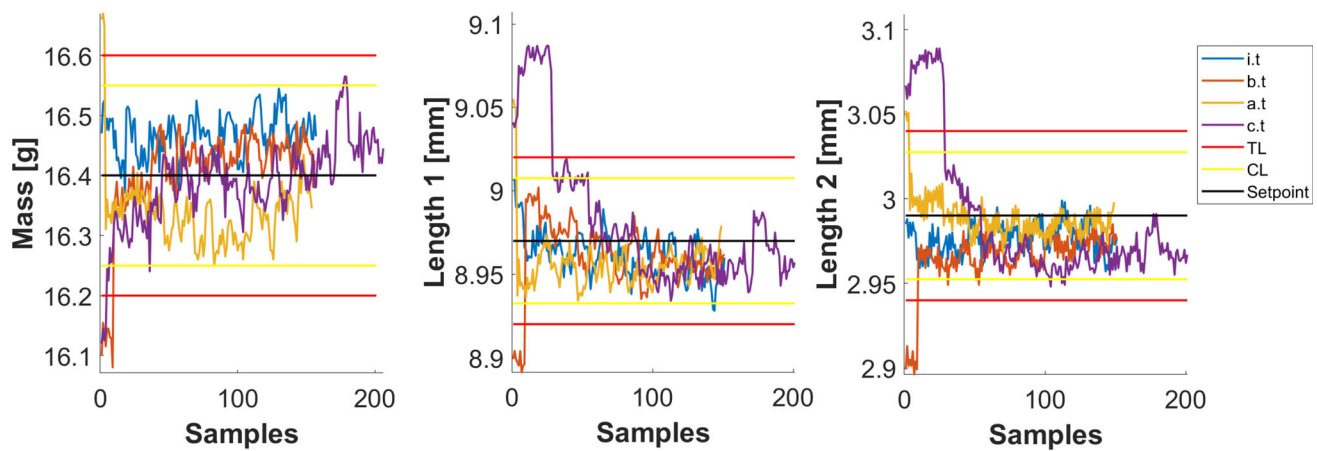


**Fig. 13** Time-series of quality characteristics of workpiece 1 for control based on neural network predictions

**Table 8** Control performance of sensor-based and NN-based control for workpiece 1

| Initial condition | Approach       | $N$ | Settling (#W) |          |          | Steady-state (RMSE) |          |          |
|-------------------|----------------|-----|---------------|----------|----------|---------------------|----------|----------|
|                   |                |     | Mass          | Length 1 | Length 2 | Mass                | Length 1 | Length 2 |
| Within            | Sensors        | 10  |               |          |          | 0.0399              | 0.0154   | 0.0116   |
|                   | Neural network | 10  |               |          |          | 0.0591              | 0.0191   | 0.0126   |
| Below             | Sensors        | 10  | 1             | 3.9      | 5.8      | 0.0421              | 0.0142   | 0.0086   |
|                   | Neural network | 10  | 1             | 1.2      | 3.5      | 0.0505              | 0.0216   | 0.0170   |
| Above             | Sensors        | 10  | 1.1           | 3.9      | 6.5      | 0.0362              | 0.0110   | 0.0070   |
|                   | Neural network | 10  | 1             | 1.1      | 1        | 0.0476              | 0.0231   | 0.0122   |
| Crossed           | Sensors        | 10  | 1.4           | 10.3     | 10.6     | 0.0482              | 0.0174   | 0.0110   |
|                   | Neural network | 10  | 1             | 4.6      | 2.8      | 0.0385              | 0.0292   | 0.0166   |
| All conditions    | Sensors        | 40  |               |          |          | 0.0416              | 0.0145   | 0.0095   |
|                   | Neural network | 40  |               |          |          | 0.0489              | 0.0232   | 0.0146   |

the quality measures, settling (#W) as well as steady-state (*RMSE*) performance for all quality characteristics.

Again, the settling performance for the different initial conditions had to be analyzed individually since averaging over all of them would have resulted in no significant differences due to the large differences in the obtained values between conditions. When analyzing the initial conditions individually though, significant results could be obtained at a 5% significance level for several of the lengths 1 to 4. Overall, the analysis indicates that the neural-network-based approach leads to a significantly better control performance for lengths when settling than the sensor-based approach. In terms of mass, no significant difference could be found for all initial conditions.

Concerning the steady-state performance, the t-test performed on the data averaged over all experiments showed significant differences at a significance level of 5% for all the quality characteristics. In terms of mass, the t-test indicated significantly better performance of the sensor-based approach compared to the neural-network-based approach.

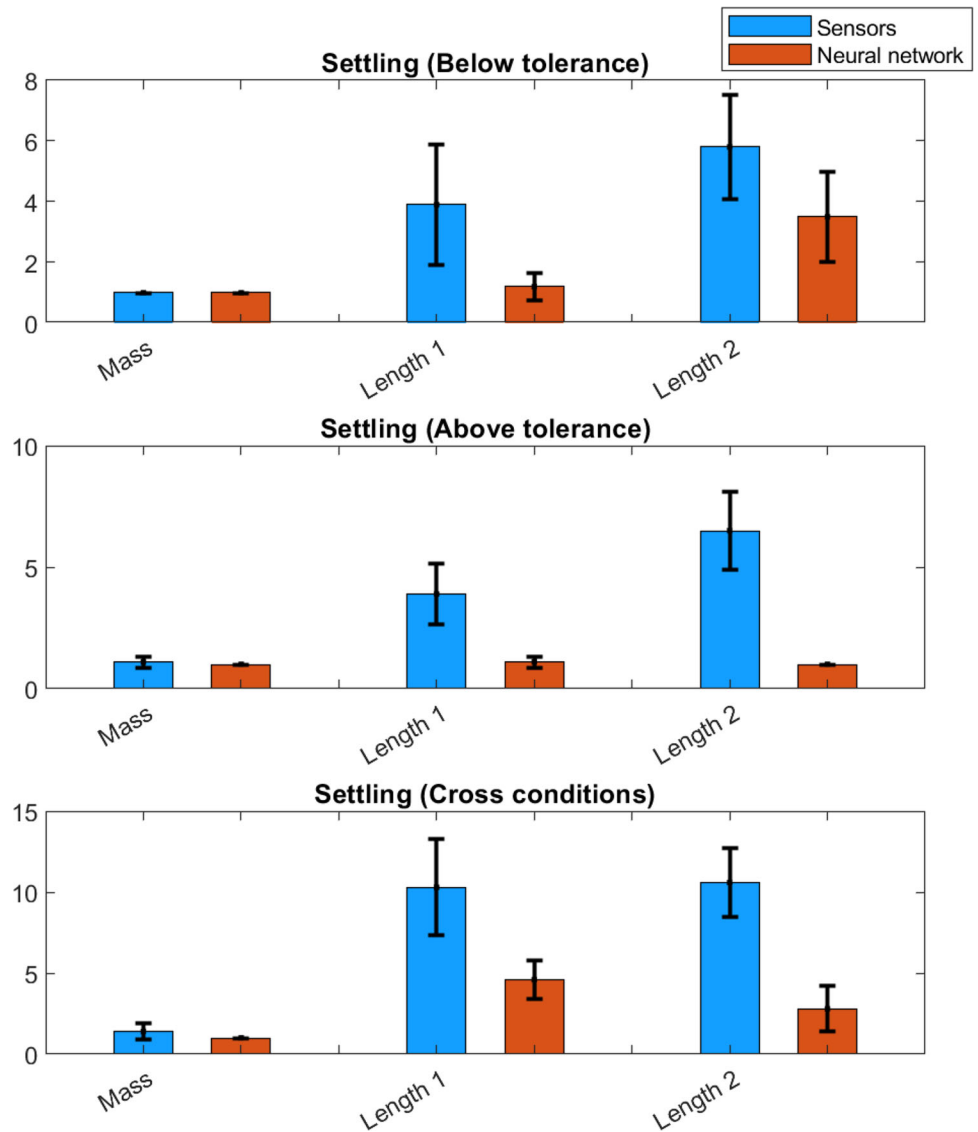
In terms of lengths 1 to 4, the t-test showed opposite results with a significantly better performance of the neural-network-based approach compared to the sensor-based approach.

## Discussion

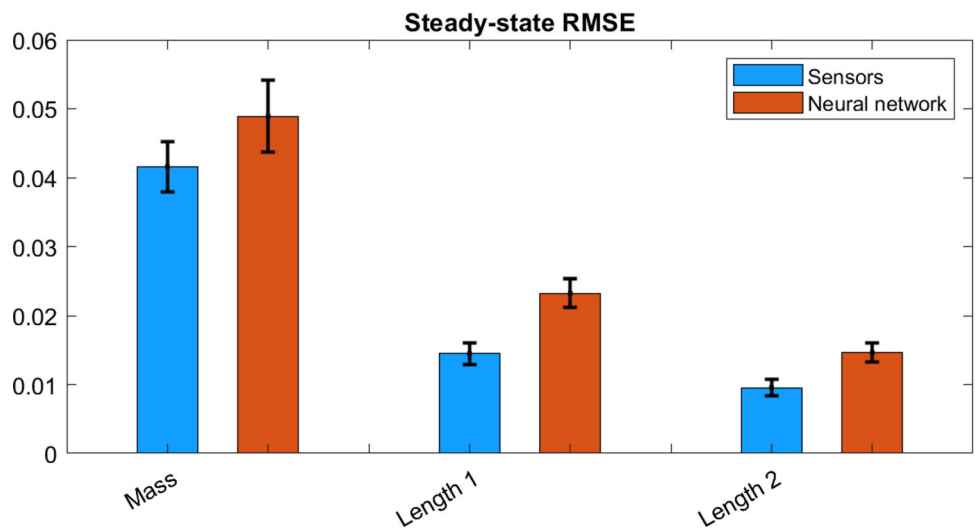
Overall, both approaches were found to be able to bring and keep quality characteristics within their tolerance limits. However, they were found to achieve this with different performances. In terms of control performance in steady-state, the sensor-based approach was found to outperform the neural-network-based approach when controlling the quality characteristics of the first workpiece. This indicates that the neural network was not able to keep up with the high accuracy of the measurement system when estimating lengths, which then compromised the control performance. The same effect was not found for the second workpiece. This can be explained by the fact that the achieved estimation performance of the neural network differs significantly between the two workpieces as can be observed in Table 12. While



**Fig. 14** Settling (means and 95 % confidence intervals) for different initial conditions for workpiece 1

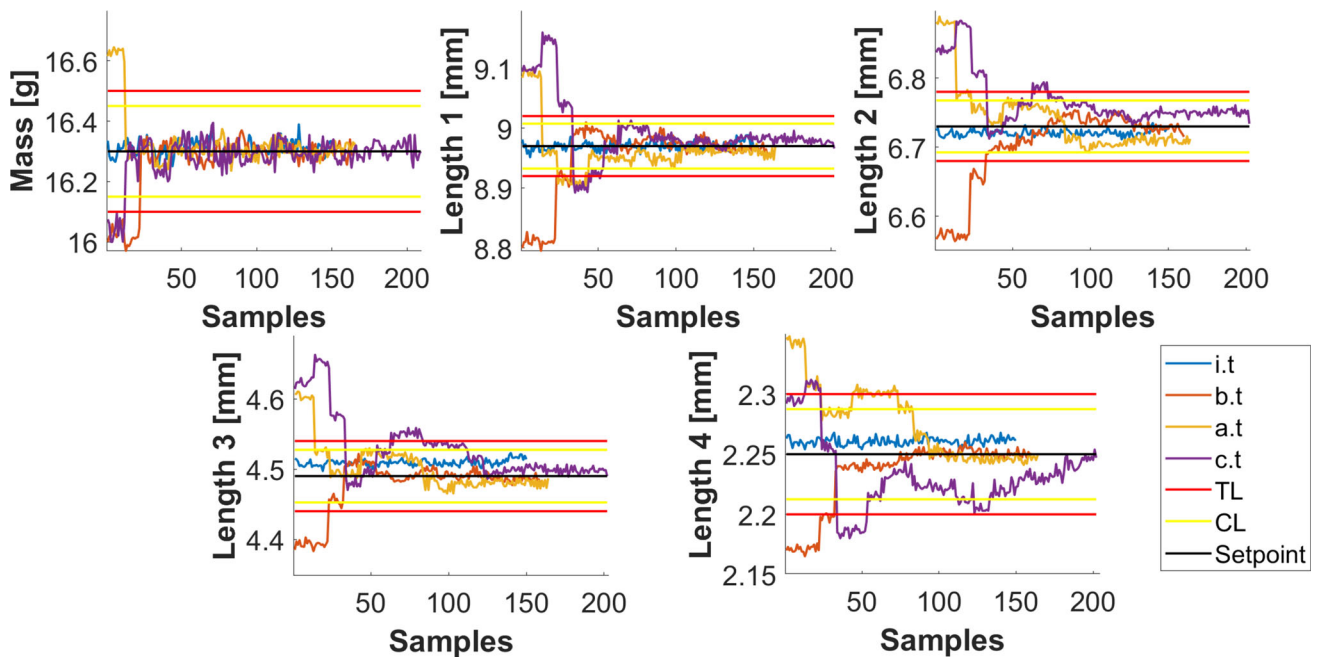


**Fig. 15** Steady-state RMSE (means and 95 % confidence intervals) for workpiece 1



**Table 9** Results of statistical analysis (t-tests) for workpiece 1

| Initial Condition | Variable          | Approach       | N  | Mean   | Std. error | t     | $\alpha$ |
|-------------------|-------------------|----------------|----|--------|------------|-------|----------|
| Below             | Settling_Mass     | Sensors        | 10 | 1      | 0          | –     | –        |
|                   |                   | Neural network | 10 | 1      | 0          |       |          |
|                   | Settling_Length 1 | Sensors        | 10 | 3.9    | 0.875      | 3.008 | 0.013    |
|                   |                   | Neural Network | 10 | 1.2    | 0.200      |       |          |
|                   | Settling_Length 2 | Sensors        | 10 | 5.8    | 0.757      | 2.299 | 0.034    |
|                   |                   | Neural network | 10 | 3.5    | 0.654      |       |          |
| Above             | Settling_Mass     | Sensors        | 10 | 1.1    | 0.100      | 1.000 | 0.343    |
|                   |                   | Neural network | 10 | 1      | 0          |       |          |
|                   | Settling_Length 1 | Sensors        | 10 | 3.9    | 0.547      | 5.038 | 0.001    |
|                   |                   | Neural network | 10 | 1.1    | 0.100      |       |          |
|                   | Settling_Length 2 | Sensors        | 10 | 6.5    | 0.703      | 7.822 | 0.001    |
|                   |                   | Neural network | 10 | 1      | 0          |       |          |
| Crossed           | Settling_Mass     | Sensors        | 10 | 1.4    | 0.221      | 1.809 | 0.104    |
|                   |                   | Neural network | 10 | 1      | 0          |       |          |
|                   | Settling_Length 1 | Sensors        | 10 | 10.3   | 1.317      | 4.025 | 0.002    |
|                   |                   | Neural network | 10 | 4.6    | 0.521      |       |          |
|                   | Settling_Length 2 | Sensors        | 10 | 10.6   | 0.933      | 6.930 | 0.001    |
|                   |                   | Neural network | 10 | 2.8    | 0.629      |       |          |
| All conditions    | RMSE_Mass         | Sensors        | 40 | 0.0416 | 0.0018     | 2.326 | 0.023    |
|                   |                   | Neural network | 40 | 0.0489 | 0.0026     |       |          |
|                   | RMSE_Length 1     | Sensors        | 40 | 0.0145 | 0.0008     | 3.723 | 0.001    |
|                   |                   | Neural network | 40 | 0.0232 | 0.0010     |       |          |
|                   | RMSE_Length 2     | Sensors        | 40 | 0.0095 | 0.0006     | 5.511 | 0.001    |
|                   |                   | Neural network | 40 | 0.0146 | 0.0007     |       |          |

**Fig. 16** Time-series of quality characteristics of workpiece 2 for sensor-based approach

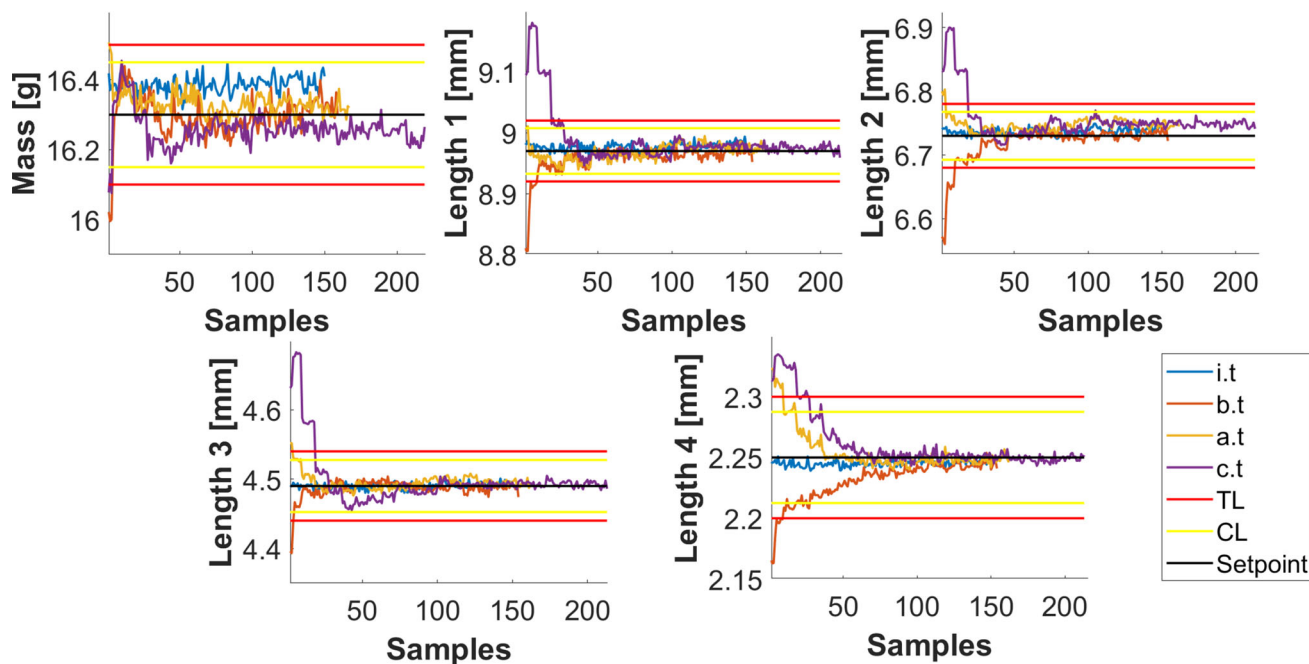


Fig. 17 Time-series of quality characteristics of workpiece 2 for neural-network-based approach

Table 10 Control performance of sensor-based and NN-based control for workpiece 2

| Initial condition | Approach       | N  | Settling (#W) |          |          |          |          | Steady-state (RMSE) |          |          |          |          |
|-------------------|----------------|----|---------------|----------|----------|----------|----------|---------------------|----------|----------|----------|----------|
|                   |                |    | Mass          | Length 1 | Length 2 | Length 3 | Length 4 | Mass                | Length 1 | Length 2 | Length 3 | Length 4 |
| Within            | Sensors        | 10 |               |          |          |          |          | 0.0296              | 0.0076   | 0.0113   | 0.0203   | 0.0097   |
|                   | Neural network | 10 |               |          |          |          |          | 0.0923              | 0.0110   | 0.0100   | 0.0060   | 0.0065   |
| Below             | Sensors        | 10 | 1.8           | 4.2      | 5.2      | 3.5      | 3.3      | 0.0265              | 0.0121   | 0.0128   | 0.0099   | 0.0065   |
|                   | Neural network | 10 | 1.1           | 1.8      | 1.9      | 1        | 4        | 0.0651              | 0.0112   | 0.0070   | 0.0072   | 0.0090   |
| Above             | Sensors        | 10 | 1.2           | 3.6      | 3        | 8.9      | 10.3     | 0.0290              | 0.0131   | 0.0180   | 0.0140   | 0.0155   |
|                   | Neural network | 10 | 1             | 1        | 1        | 1        | 2        | 0.0473              | 0.0085   | 0.0077   | 0.0059   | 0.0096   |
| Crossed           | Sensors        | 10 | 1.6           | 8.5      | 10.4     | 12.9     | 8.1      | 0.0348              | 0.0139   | 0.0175   | 0.0232   | 0.0105   |
|                   | Neural network | 10 | 1             | 3.9      | 3        | 2.9      | 4.8      | 0.0695              | 0.0096   | 0.0191   | 0.0064   | 0.0045   |
| All conditions    | Sensors        | 40 |               |          |          |          |          | 0.0300              | 0.0117   | 0.0149   | 0.0168   | 0.0106   |
|                   | Neural network | 40 |               |          |          |          |          | 0.0685              | 0.0101   | 0.0109   | 0.0064   | 0.0074   |

quite low estimation errors could be achieved for the second workpiece, for the first one the estimation errors were higher. Thus, the neural networks of the first workpiece would need to be updated to be able to reach the accuracy of the sensor-based approach.

What concerns the control performance in the transient phase, the neural-network-based approach was found to outperform the sensor-based approach for lengths. This can be explained by the fact that the neural-network-based approach is able to overcome the problem with the delayed measurement by the triangulation sensor and thus, can react quicker and achieve a better control performance than the sensor-based approach. Overall, the neural-network-based approach

turned out to be best when controlling lengths in the transient phase.

In terms of controlling mass in the transient phase, no significant differences could be found. This can be explained by the fact that the measurement of the mass, unlike lengths, is not delayed much; thus, estimators could not really bring an advantage compared to the sensor-based approach. Overall, both approaches could be equally used for controlling mass in the transient phase.

**Table 11** Results of statistical analysis (t-tests) for workpiece 2

| Initial Condition | Variable          | Approach       | N      | Mean   | Std. error | <i>t</i> | $\alpha$ |
|-------------------|-------------------|----------------|--------|--------|------------|----------|----------|
| Below             | Settling_Mass     | Sensors        | 10     | 1.8    | 0.326      | 2.049    | 0.066    |
|                   |                   | Neural network | 10     | 1.1    | 0.100      |          |          |
|                   | Settling_Length 1 | Sensors        | 10     | 4.2    | 0.326      | 4.536    | 0.001    |
|                   |                   | Neural Network | 10     | 1.8    | 0.416      |          |          |
|                   | Settling_Length 2 | Sensors        | 10     | 5.2    | 0.680      | 4.165    | 0.001    |
|                   |                   | Neural network | 10     | 1.9    | 0.407      |          |          |
|                   | Settling_Length 3 | Sensors        | 10     | 3.5    | 0.373      | 6.708    | 0.001    |
|                   |                   | Neural network | 10     | 1      | 0          |          |          |
| Settling_Length 4 | Sensors           | 10             | 3.3    | 0.396  | 1.172      | 0.257    |          |
|                   | Neural network    | 10             | 4      | 0.447  |            |          |          |
| Above             | Settling_Mass     | Sensors        | 10     | 1.200  | 0.133      | 1.500    | 0.168    |
|                   |                   | Neural network | 10     | 1      | 0          |          |          |
|                   | Settling_Length 1 | Sensors        | 10     | 3.600  | 0.733      | 3.545    | 0.006    |
|                   |                   | Neural network | 10     | 1      | 0          |          |          |
|                   | Settling_Length 2 | Sensors        | 10     | 3.000  | 0.365      | 5.477    | 0.001    |
|                   |                   | Neural network | 10     | 1      | 0          |          |          |
|                   | Settling_Length 3 | Sensors        | 10     | 8.900  | 0.936      | 8.437    | 0.001    |
|                   |                   | Neural network | 10     | 1      | 0          |          |          |
| Settling_Length 4 | Sensors           | 10             | 10.300 | 1.468  | 5.652      | 0.001    |          |
|                   | Neural network    | 10             | 2      | 0      |            |          |          |
| Crossed           | Settling_Mass     | Sensors        | 10     | 1.600  | 0.305      | 1.964    | 0.081    |
|                   |                   | Neural network | 10     | 1      | 0          |          |          |
|                   | Settling_Length 1 | Sensors        | 10     | 8.500  | 1.067      | 3.807    | 0.002    |
|                   |                   | Neural network | 10     | 3.9    | 0.567      |          |          |
|                   | Settling_Length 2 | Sensors        | 10     | 10.400 | 0.945      | 7.225    | 0.001    |
|                   |                   | Neural network | 10     | 3      | 0.394      |          |          |
|                   | Settling_Length 3 | Sensors        | 10     | 12.900 | 1.946      | 5.015    | 0.001    |
|                   |                   | Neural network | 10     | 2.9    | 0.433      |          |          |
| Settling_Length 4 | Sensors           | 10             | 8.1    | 1.120  | 2.569      | 0.022    |          |
|                   | Neural network    | 10             | 4.8    | 0.629  |            |          |          |
| All conditions    | RMSE_Mass         | Sensors        | 40     | 0.0299 | 0.0015     | 8.663    | 0.001    |
|                   |                   | Neural network | 40     | 0.0685 | 0.0042     |          |          |
|                   | RMSE_Length 1     | Sensors        | 40     | 0.0117 | 0.0007     | 2.027    | 0.047    |
|                   |                   | Neural network | 40     | 0.0101 | 0.0004     |          |          |
|                   | RMSE_Length 2     | Sensors        | 40     | 0.0149 | 0.0011     | 2.792    | 0.007    |
|                   |                   | Neural network | 40     | 0.0109 | 0.0009     |          |          |
|                   | RMSE_Length 3     | Sensors        | 40     | 0.0168 | 0.0015     | 6.992    | 0.001    |
|                   |                   | Neural network | 40     | 0.0064 | 0.0003     |          |          |
| RMSE_Length 4     | Sensors           | 40             | 0.0105 | 0.0012 | 2.341      | 0.023    |          |
|                   | Neural network    | 40             | 0.0074 | 0.0005 |            |          |          |

## Conclusion

We presented an approach that allows adjusting trajectory key points and with this the final piston trajectories of a compaction press to bring and keep quality characteristics like mass and dimensions within tolerance. The quality characteristics of two multi-level workpieces were controlled in a

cascaded fashion by concentrating on one quality characteristic at a time. To reduce costs for expensive sensors we introduced neural networks for the estimation of the quality characteristics and compared their performance to the baseline based on sensor measurements. We finally compared the performance of the closed-loop controllers when based on sensor measurements and neural network predictions.

**Fig. 18** Settling (means and 95 % confidence intervals) for different initial conditions for workpiece 2

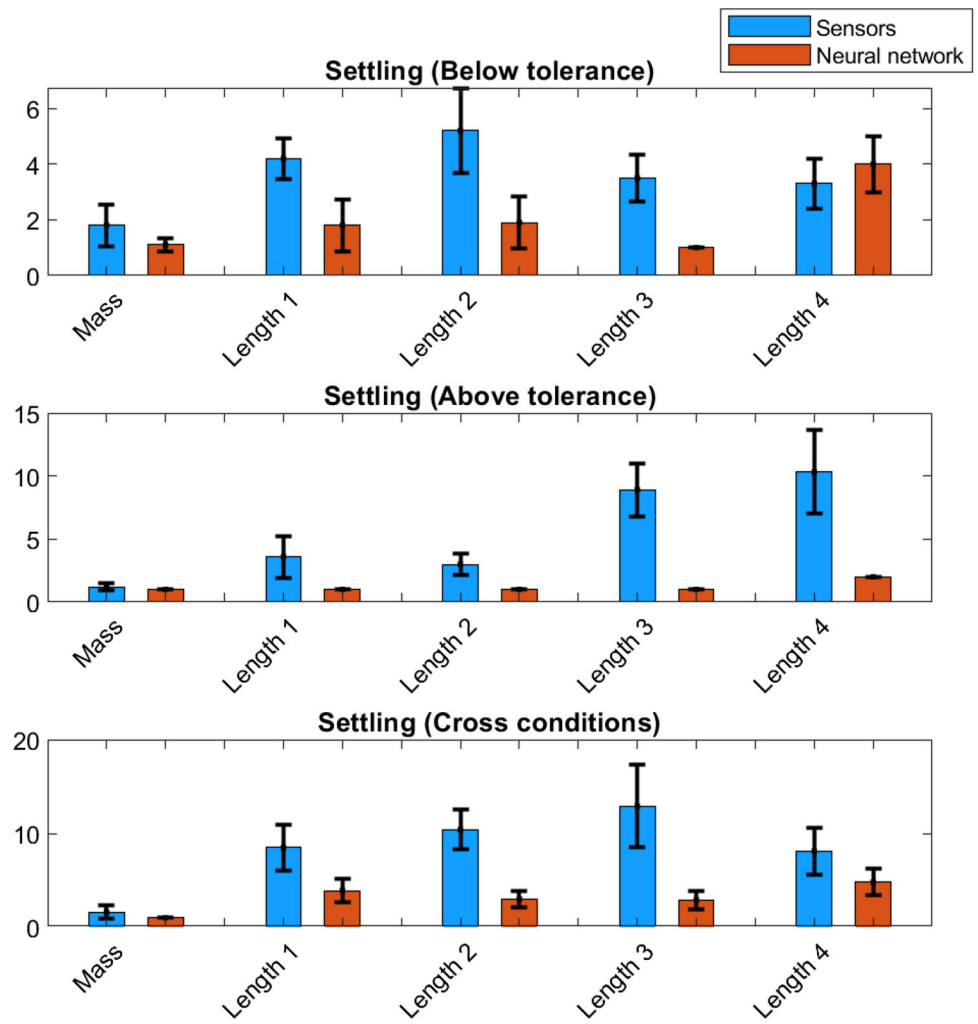


**Fig. 19** Steady-stat RMSE (means and 95 % confidence intervals) for workpiece 2

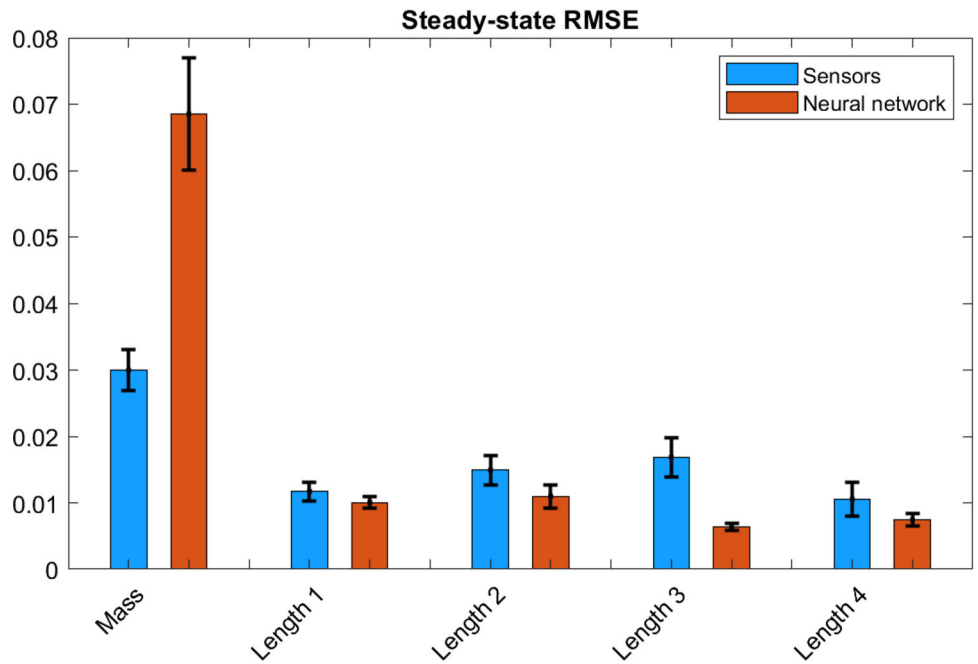


**Table 12** Comparison of the steady-state RMSE and estimation RMSE for both workpieces

| Steady-state RMSE |          |          |          |          | Estimation RMSE |          |          |          |          |
|-------------------|----------|----------|----------|----------|-----------------|----------|----------|----------|----------|
| Workpiece 1       |          |          |          |          |                 |          |          |          |          |
| Mass              | Length 1 | Length 2 |          |          | Mass            | Length 1 | Length 2 |          |          |
| 0.0489            | 0.0232   | 0.0146   |          |          | 0.0470          | 0.0204   | 0.0122   |          |          |
| Workpiece 2       |          |          |          |          |                 |          |          |          |          |
| Mass              | Length 1 | Length 2 | Length 3 | Length 4 | Mass            | Length 1 | Length 2 | Length 3 | Length 4 |
| 0.0685            | 0.0101   | 0.0109   | 0.0064   | 0.0074   | 0.0652          | 0.0084   | 0.0099   | 0.0060   | 0.0073   |

Overall, both approaches were found to be able to bring and keep all quality characteristics within their tolerance limits. However, they were found to achieve this with different performances. Results indicated that the neural-network-based approach outperformed the sensor-based approach for the transient phase, whereas the neural networks needed to be updated from time to time in order to be able to compete with the sensor-based approach in terms of predicting the steady state. For this reason, an algorithm was presented that runs in real-time and updates the network models. The results showed that for the updated version of models, the steady-state errors could be eliminated. Since updating needs to be performed only from time to time, required sensors like the expensive triangulation sensors can be shared among multiple machines and thus, costs can be reduced. At the same time the superior prediction performance of the neural-network-based approach in transient phases can be exploited to accelerate setting up times for new workpieces.

The presented work requires a rich database to train the neural network models effectively. In this paper, we manually changed the press settings in a random fashion and passed them to the control law to generate a training dataset. However, a better approach would foresee the implementation of an algorithm that automatically generates a training dataset that adequately covers the prediction space in a safe way. Another limitation lies in the extension of the presented method to more complex workpieces. The challenge hereby arises from the laser triangulation sensor, as measuring various dimensions becomes increasingly complex with more intricate shapes. Another future direction, could foresee adding extra sensor information from temperature and humidity sensors. This would increase the number of inputs for the neural network models and could help improving the accuracy of the estimations. Furthermore, in addition to neural networks, the efficacy of other advanced machine learning algorithms for estimating the quality characteristics could be investigated. A comprehensive comparison of these algorithms will provide valuable insights into which approach yields the best accuracy and robustness for our specific application. Finally, another intriguing avenue for future research

involves also exploring the combination of sensor measurements and neural network estimations.

**Author Contributions** This work was supported by the Open Access Publishing Fund provided by the Free University of Bozen-Bolzano. All authors contributed to the study conception and design. Material preparation and data collection were performed by Hoomaan MoradiMaryamnegari, Elias Ganthaler, and Thomas Villgratner and its analysis by Hoomaan MoradiMaryamnegari, Seif-El-Islam-Hasseni, Elias Ganthaler, and Angelika Peer. The first draft of the manuscript was written by Hoomaan MoradiMaryamnegari and all authors commented on the versions of the manuscript. All authors read and approved the final manuscript.

**Funding** This work was supported in part by the 'RobuSinter' project funded by the European Regional Development Fund (ERDF), project No. 1113.

**Data Availability** The datasets generated and analysed during the current study are not publicly available due the fact that they fall within the items regulated by a nondisclosure agreement signed with the involved company.

## Declarations

**Competing interests** The authors have no competing interests to declare that are relevant to the content of this article.

**Open Access** This article is licensed under a Creative Commons Attribution 4.0 International License, which permits use, sharing, adaptation, distribution and reproduction in any medium or format, as long as you give appropriate credit to the original author(s) and the source, provide a link to the Creative Commons licence, and indicate if changes were made. The images or other third party material in this article are included in the article's Creative Commons licence, unless indicated otherwise in a credit line to the material. If material is not included in the article's Creative Commons licence and your intended use is not permitted by statutory regulation or exceeds the permitted use, you will need to obtain permission directly from the copyright holder. To view a copy of this licence, visit <http://creativecommons.org/licenses/by/4.0/>.

## References

- Beiss, P. (2013). *Pulvermetallurgische Fertigungstechnik* (1st ed.). Berlin, Heidelberg: Springer Vieweg. <https://doi.org/10.1007/978-3-642-32032-3>



- Evans, J. W., & De Jonghe, L. C. (2016). Powder Compaction. In *The Production and Processing of Inorganic Materials*. The Minerals, Metals, and Materials Series (MMMS), Springer, Cham, p. 383–401. [https://doi.org/10.1007/978-3-319-48163-0\\_12](https://doi.org/10.1007/978-3-319-48163-0_12).
- Ganthaler, E., MoradiMaryamnegari, H., Villgratner, T., et al. (2023). Automatic trajectory adaptation for the control of quality characteristics in a powder compaction process. *Journal of Manufacturing Processes*, 107, 268–279. <https://doi.org/10.1016/j.jmapro.2023.09.060>
- Klocke, F. (2015). *Fertigungsverfahren 5* (4th ed.). Berlin, Heidelberg: Springer Vieweg. <https://doi.org/10.1007/978-3-540-69512-7>
- Koutsoupakis, J., Seventekidis, P., & Giagopoulos, D. (2023). Machine learning based condition monitoring for gear transmission systems using data generated by optimal multibody dynamics models. *Mechanical Systems and Signal Processing*, 190, 110130. <https://doi.org/10.1016/J.YMSSP.2023.110130>
- Krok, A., & Wu, C. Y. (2017). Finite element modeling of powder compaction. NATO Science for Peace and Security Series A: Chemistry and Biology, vol. PartF1. Springer Verlag, p 451–462. [https://doi.org/10.1007/978-94-024-1117-1\\_28/COVER](https://doi.org/10.1007/978-94-024-1117-1_28/COVER).
- Kumar, N., Bharti, A., & Dixit, M. (2021). Powder Compaction Dies and Compressibility of Various Materials. *Powder Metallurgy and Metal Ceramics*, 60(7–8), 403–409. <https://doi.org/10.1007/S11106-021-00253-X/METRICS>
- Liu, J., Ye, J., Izquierdo, D. S., et al. (2023). A review of machine learning techniques for process and performance optimization in laser beam powder bed fusion additive manufacturing. *Journal of Intelligent Manufacturing*, 34, 3249–3275. <https://doi.org/10.1007/s10845-022-02012-0>
- Li, C., Wu, B., Zhang, Z., et al. (2022). A novel process planning method of 3 + 2-axis additive manufacturing for aero-engine blade based on machine learning. *Journal of Intelligent Manufacturing*, 34(4), 2027–2042. <https://doi.org/10.1007/S10845-021-01898-6/FIGURES/17>
- Long, X. Y., Zhao, S. K., Jiang, C., et al. (2021). Deep learning-based planar crack damage evaluation using convolutional neural networks. *Engineering Fracture Mechanics*, 246, 107604. <https://doi.org/10.1016/J.ENGFRACMECH.2021.107604>
- Lou, H., Chung, J. I., Kiang, Y. H., et al. (2019). The application of machine learning algorithms in understanding the effect of core/shell technique on improving powder compactability. *International Journal of Pharmaceutics*, 555, 368–379. <https://doi.org/10.1016/J.IJPHARM.2018.11.039>
- Malik, A. R., Pani, B. B., Badjena, S. K., et al. (2022). Prediction of powder metallurgy process parameters for ferrous based materials by artificial neural network technique. *Materials Today: Proceedings*, 62, 4432–4435. <https://doi.org/10.1016/J.MATPR.2022.04.905>
- Manivannan, S., Biswas, P., Barick, P., et al. (2021). Comparative Study on Compaction and Sintering Behavior of Spray and Freeze Granulated Magnesium Aluminate Spinel Powder. *Transactions of the Indian Ceramic Society*, 80(2), 110–117. <https://doi.org/10.1080/0371750X.2021.1887765>
- Massimo, D., Ganthaler, E., Buriro, A., et al. (2023). Estimation of mass and lengths of sintered workpieces using machine learning models. *IEEE Transactions on Instrumentation and Measurement*, 72, 1–14. <https://doi.org/10.1109/TIM.2023.3298413>
- O'Flynn, J., & Corbin, S. F. (2019). Effects of powder material and process parameters on the roll compaction, sintering and cold rolling of titanium sponge. *Powder Metallurgy*, 62(5), 307–321. <https://doi.org/10.1080/00325899.2019.1651505>
- Qin, Y., Liu, X., Yue, C., et al. (2023). Tool wear identification and prediction method based on stack sparse self-coding network. *Journal of Manufacturing Systems*, 68, 72–84. <https://doi.org/10.1016/J.JMSY.2023.02.006>
- Satterlee, N., Torresani, E., Olevsky, E., et al. (2022). Comparison of machine learning methods for automatic classification of porosities in powder-based additive manufactured metal parts. *International Journal of Advanced Manufacturing Technology*, 120(9–10), 6761–6776. <https://doi.org/10.1007/S00170-022-09141-Z/METRICS>
- Schatt, W., Wieters, K., & Kieback, B. (2007). Prüfung und Charakterisierung der Pulver. In *Pulvermetallurgie*. Springer, Berlin, Heidelberg, p 71–110. [https://doi.org/10.1007/978-3-540-68112-0\\_4](https://doi.org/10.1007/978-3-540-68112-0_4).
- Sivasankaran, S., Sivaprasad, K., & Narayanasamy, R., et al. (2011). Evaluation of compaction equations and prediction using adaptive neuro-fuzzy inference system on compressibility behavior of AA 6061<sub>100-x</sub>–x wt.% TiO<sub>2</sub> nanocomposites prepared by mechanical alloying. *Powder Technology*, 209(1–3), 124–137. <https://doi.org/10.1016/J.POWTEC.2011.02.020>
- van der Haven, D. L., Ørtoft, F. H., Naelapää, K., et al. (2022). Predictive modelling of powder compaction for binary mixtures using the finite element method. *Powder Technology*, 403, 117381. <https://doi.org/10.1016/J.POWTEC.2022.117381>
- Wang, C., Wang, J. H., Gu, S. S., et al. (2017). Elongation prediction of steel-strips in annealing furnace with deep learning via improved incremental extreme learning machine. *International Journal of Control, Automation and Systems*, 15(3), 1466–1477. <https://doi.org/10.1007/S12555-015-0463-7/METRICS>
- Wilson, D., Roberts, R., & Blyth, J. (2019). *Powder Compaction: Process Design and Understanding* (pp. 203–225). Hoboken, USA: John Wiley & Sons Ltd. <https://doi.org/10.1002/9781119600800.ch59>
- Yu Pimenov, D., Bustillo, A., Wojciechowski, S., et al. (2022). Artificial intelligence systems for tool condition monitoring in machining: analysis and critical review. *Journal of Intelligent Manufacturing*, 34(5), 2079–2121. <https://doi.org/10.1007/S10845-022-01923-2>

**Publisher's Note** Springer Nature remains neutral with regard to jurisdictional claims in published maps and institutional affiliations.